Research Article | Vol. 25, No. 3 | 6 Feb 2017 | OPTICS EXPRESS 2130

Optics EXPRESS

See-through near-eye displays enabling vision correction

LEI ZHOU, CHAO PING CHEN,* YISHI WU, ZHONGLIN ZHANG, KEYU WANG, BING YU, AND YANG LI

Smart Display Lab, Department of Electronic Engineering, Shanghai Jiao Tong University, Shanghai, China
**ccp@sjtu.edu.cn*

Abstract: We propose a see-through near-eye display, which is dedicated to the visually impaired users who suffer from refractive anomalies. Our solution is characterized by a pair of corrective lenses coated with multiplexed volume holograms. Its key performance including diffraction efficiency, field of view, modulation transfer function, and distortion has been studied.

OCIS codes: (090.2820) Heads-up displays; (080.2740) Geometric optical design; (120.2040) Displays.

References and links

1. R. Azuma, Y. Baillot, R. Behringer, S. Feiner, S. Julier, and B. MacIntyre, "Recent advances in augmented reality," IEEE Comput. Graph. **21**(6), 34–47 (2001).
2. Y. Amitai, "Extremely compact high-performance HMDs based on substrate-guided optical element," *SID Symposium* (2004), pp. 310–313.
3. H. Mukawa, K. Akutsu, I. Matsumura, S. Nakano, T. Yoshida, M. Kuwahara, and K. Aiki, "A full-color eyewear display using planar waveguides with reflection volume holograms," J. Soc. Inf. Disp. **17**(3), 185–193 (2009).
4. Z. Wu, J. Liu, and Y. Wang, "A high-efficiency holographic waveguide display system with a prism in-coupler," J. Soc. Inf. Disp. **21**(12), 524–528 (2013).
5. C. P. Chen, S. P. Preman, T.-H. Yoon, and J. C. Kim, "Dual-mode operation of dual-frequency liquid crystal cell by horizontal switching," Appl. Phys. Lett. **92**(12), 123505 (2008).
6. B. A. Holden, T. R. Fricke, D. A. Wilson, M. Jong, K. S. Naidoo, P. Sankaridurg, T. Y. Wong, T. J. Naduvilath, and S. Resnikoff, "Global prevalence of myopia and high myopia and temporal trends from 2000 through 2050," Ophthalmology **123**(5), 1036–1042 (2016).
7. Y. Amitai, S. Reinhorn, and A. A. Friesem, "Visor-display design based on planar holographic optics," Appl. Opt. **34**(8), 1352–1356 (1995).
8. K. Kiyokawa, Y. Kurata, and H. Ohno, "An optical see-through display for mutual occlusion with a real-time stereovision system," Comput. Graph. **25**(5), 765–779 (2001).
9. O. Cakmakci and J. Rolland, "Head-worn displays: a review," J. Disp. Technol. **2**(3), 199–216 (2006).
10. A. Cameron, "The application of holographic optical waveguide technology to the Q-Sight family of helmet-mounted displays," Proc. SPIE **7326**, 73260H (2009).
11. D. Cheng, Y. Wang, H. Hua, and M. M. Talha, "Design of an optical see-through head-mounted display with a low f-number and large field of view using a freeform prism," Appl. Opt. **48**(14), 2655–2668 (2009).
12. Q. Wang, D. Cheng, Y. Wang, H. Hua, and G. Jin, "Design, tolerance, and fabrication of an optical see-through head-mounted display with free-form surface elements," Appl. Opt. **52**(7), C88–C99 (2013).
13. H. Hua, "Past and future of wearable augmented reality displays and their applications," Proc. SPIE **9186**, 91860O (2014).
14. D. Cheng, Y. Wang, C. Xu, W. Song, and G. Jin, "Design of an ultra-thin near-eye display with geometrical waveguide and freeform optics," Opt. Express **22**(17), 20705–20719 (2014).
15. H.-S. Chen, Y.-J. Wang, P.-J. Chen, and Y.-H. Lin, "Electrically adjustable location of a projected image in augmented reality via a liquid-crystal lens," Opt. Express **23**(22), 28154–28162 (2015).
16. J. Han, J. Liu, X. Yao, and Y. Wang, "Portable waveguide display system with a large field of view by integrating freeform elements and volume holograms," Opt. Express **23**(3), 3534–3549 (2015).
17. B. Kress, V. Raulot, and M. Grossman, "Exit pupil expander for wearable see-through displays," Proc. SPIE **8368**, 83680D (2012).
18. A. G. Taylor, *Develop Microsoft HoloLens Apps Now* (Apress, 2016).
19. R. B. Sprague, "Method and apparatus to process display and non-display information," US Patent 8,520,309 B2 (2008).
20. M. S. Brennesholtz and E. H. Stupp, *Projection Displays 2nd Edition* (Wiley, 2008).
21. F. L. Pedrotti, L. M. Pedrotti, and L. S. Pedrotti, *Introduction to Optics 3rd Edition* (Addison-Wesley, 2006).

#283180 http://dx.doi.org/10.1364/OE.25.002130
Journal © 2017 Received 19 Dec 2016; revised 19 Jan 2017; accepted 20 Jan 2017; published 25 Jan 2017

Optics EXPRESS

22. R. Bräuer and O. Bryngdahl, "Electromagnetic diffraction analysis of two-dimensional gratings," Opt. Commun. **100**(1-4), 1–5 (1993).
23. E. Noponen and J. Turunen, "Eigenmode method for electromagnetic synthesis of diffractive elements with three-dimensional profiles," J. Opt. Soc. Am. A **11**(9), 2494–2502 (1994).
24. L. Li, "New formulation of the Fourier modal method for crossed surface-relief gratings," J. Opt. Soc. Am. A **14**(10), 2758–2767 (1997).
25. R. Shi, J. Liu, H. Zhao, Z. Wu, Y. Liu, Y. Hu, Y. Chen, J. Xie, and Y. Wang, "Chromatic dispersion correction in planar waveguide using one-layer volume holograms based on three-step exposure," Appl. Opt. **51**(20), 4703–4708 (2012).
26. H. Kogelnik, "Coupled wave theory for thick hologram gratings," Bell Syst. Tech. J. **48**(9), 2909–2947 (1969).
27. R. E. Fischer, B. Tadic-Galeb, and P. R. Yoder, *Optical System Design 2nd Edition* (McGraw-Hill Education, 2008).

1. Introduction

Augmented reality (AR) [1] is a technology that merges the digital information with the real world in real time. See-through near-eye display (NED) [2–4] is a key component of AR, through which the computer-generated images or videos are displayed on top of the existing environment. Unlike flat panel displays, such as liquid crystal display [5], NED is wearable and very close to the eyes. Therefore, not just the optical performance of the displays but also the vision acuity of the users needs to be considered. According to a recent study on the global prevalence of myopia—also known as nearsightness—half of the world's population will be nearsighted by 2050 [6]. Unfortunately, with current NED solutions [7–16], users, who are more or less visually impaired, are required to wear extra eyeglasses. If doing so, both the user experience and device performance will be deteriorated, as the device becomes bulky and the eyes are further from the exit pupil [17]. Microsoft's Hololens [18], among others, is such an example for being not quite friendly to visually impaired users. They have to squeeze their eyeglasses into the headset and worry about the deformation and scratch. The worse thing is that the image they see is sometimes not as big as the one seen by eyeglasses-less users. This is because part of the field of view (FOV) would be blocked by the frames of both Hololens and eyeglasses. As an alternative, users can choose to wear contact lens or even contact-lens-like NED [19]. But for aged people, it might not be a wise option for their eyes are dry and the removal of the contact lens is inconvenient.

Motivated by the above issue, we propose a compact design of see-through NED, which features a pair of corrective lenses coated with multiplexed volume holograms. With this design, for those who have refractive anomalies—e.g. myopia and hyperopia—extra eyeglasses or contact lens are no more needed. Based on numerical simulations, its FOV, modulation transfer function (MTF), and distortion have been evaluated.

2. Operational principle

2.1 Proposed structure

Figure 1 outlines the structure of the proposed monocular see-through NED, where θ is an angle intersected by the central or optical axis of the corrective lens and that of the projection lens, s_2 is the distance between the projection lens and corrective lens, and s_3 is the distance between the corrective lens and eye. The pico projector consists of a micro-display and a 4-element projection lens [20], as depicted in Fig. 2. The corrective lens is used for compensating the refractive anomalies of the eyes. They can come in a variety of shapes and designs, depending on the visual acuity and preference of the user. By way of example, a divergent lens with negative power for correcting the myopia is adopted. The volume hologram is coated on the inner surface of the corrective lens in order to reflect the light toward the eye. Alternatively, it can be also coated on the outer surface of the corrective lens.

Optics EXPRESS

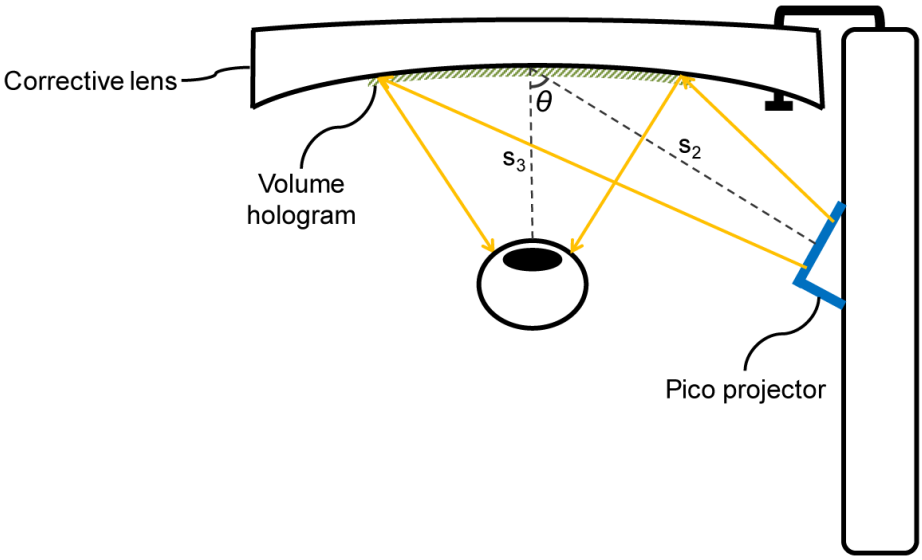

Fig. 1. Schematic drawing of the proposed monocular see-through NED. θ is an angle intersected by the central or optical axis of volume hologram and that of the projection lens, s_2 is the distance between the projection lens and corrective lens, and s_3 is the distance between the corrective lens and eye.

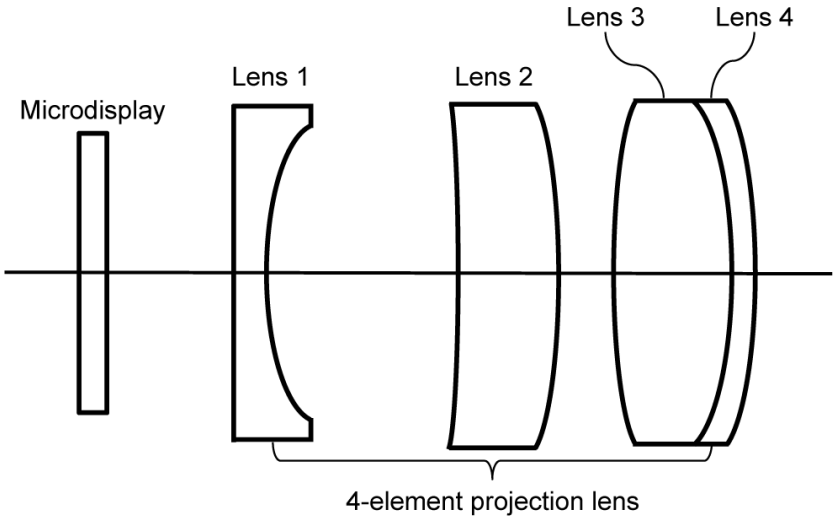

Fig. 2. Schematic drawing of the pico projector. The pico projector consists of a micro-display and a 4-element projection lens.

2.2 Design rules

Since the potential users of NEDs are most likely nearsighted, the design rules for the case of myopia are to be explained. By unfolding the optical paths from Figs. 1 & 2, the equivalent, coaxial optical path diagrams for the real and virtual images are illustrated by Figs. 3(a) and 3(b), respectively, where the 4-element projection lens is briefly described as a single lens for the sake of clarity. For the real image, light rays emitting from the real object should be diverged by a corrective lens before arriving the eyes. The diopter or optical power P_c of the corrective lens is related to the visual acuity and it can be obtained directly from the eyeglass

Optics EXPRESS

prescription. The design of the corrective lens shall follow from the lensmaker's equation [21], as given by Eq. (1)

$$P_c = \frac{1}{f_c} = \frac{n_c - n_{air}}{n_{air}}\left(\frac{1}{R_1} - \frac{1}{R_2}\right) \tag{1}$$

where f_c is the focal length of corrective lens, n_c and n_{air}, in turn, denote the refractive indices of corrective lens and air, and R_1 and R_2 are the radii of curvature of first and second surfaces of the corrective lens, respectively. In order to be consistent with Eq. (1), spherical surfaces are adopted for the corrective lens. For the virtual image, light rays emitting from the microdisplay will be first converged by the projection lens, forming an intermediate magnified virtual image S′, and then be reflected by the volume grating, which is regarded as a spherical mirror, forming the final magnified virtual image S″ received by the eyes. The distance s', defined as the distance between the image S′ and projection lens, can be determined from the thin-lens equation [21] as

$$s' = \frac{s_1}{P_p s_1 - 1} \tag{2}$$

where s_1 is the distance between the microdisplay and projection lens, and P_p is the diopter of projection lens. Similarly, the distance s'', defined as the distance between the image S″ and eye, can be derived as

$$s'' = \frac{\left(s_1 + P_p s_1 s_2 - s_2\right) R_2}{2s_1 + 2P_p s_1 s_2 - 2s_2 - P_p s_1 R_2 + R_2} \tag{3}$$

The lateral magnification m—defined as the ratio of lateral size of S″ to lateral size of microdisplay—can be written as

$$m = \frac{R_2}{2s_1 + 2P_p s_1 s_2 - 2s_2 - P_p s_1 R_2 + R_2} \tag{4}$$

To sum up, our design rules involve the following steps. First, determine the diopter of corrective lens. Second, specify the surface shapes and refractive index of corrective lens using Eq. (1). Third, determine the target value of image distance and predefine the positions of each component. Fourth, calculate the diopter of projection lens using Eq. (3). Fifth, set up the target value of one or more constraints—*e.g.* effective focal length, distortion etc.—and perform the optimization for all variables. Sixth, evaluate the performance. Apart from myopia, the above design rules can be applied to hyperopia as well. In this case, without changing correction lens' second surface, we only need to re-design its first surface to produce positive power. As for astigmatism, correction lens needs to be cylindrical [21].

Optics EXPRESS

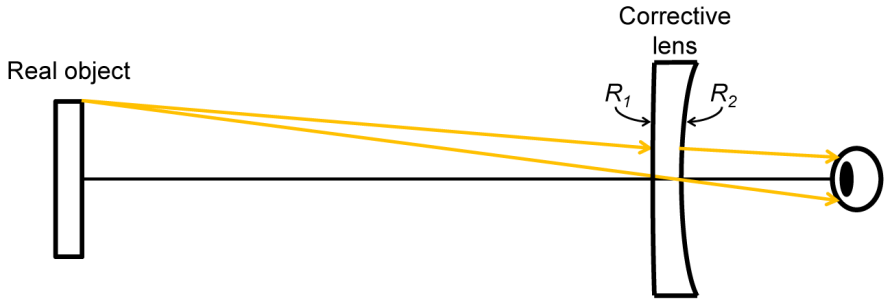

(a)

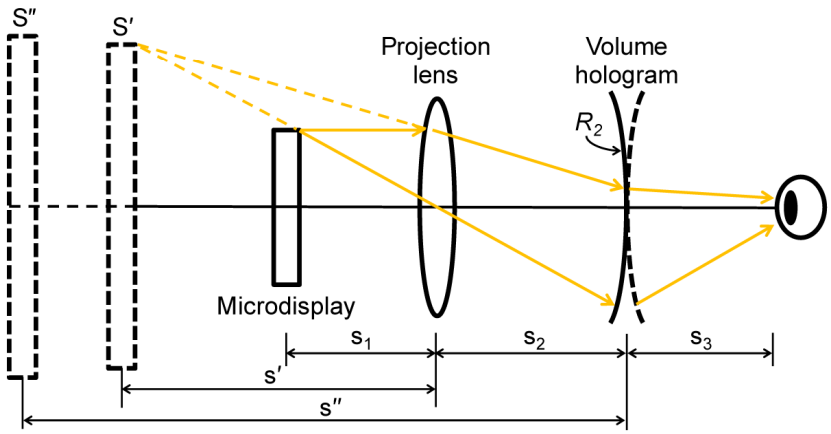

(b)

Fig. 3. Unfolded optical path diagrams for the (a) real and (b) virtual images. The 4-element projection lens is briefly described as a single lens for the sake of clarity.

2.3 Corrective lens

Consider a case that the user has only 3 diopters of myopia, disregarding the astigmatism and other types of refractive anomalies. The material of lens is chosen as the polycarbonate, which is predominantly used for eyeglasses. The shape of lens is meniscus, which has a steeper concave surface and a thinner thickness at the center than at the periphery. Compared to plano-concave and biconcave, meniscus is more acceptable for the consumer market for both aesthetic and weight reasons [22]. Our design wavelength is set as 532 nm. Following the above design rules, a corrective lens can be designed using the parameters as given in Table 1.

Table 1. Parameters used for the corrective lens

Object	Parameter	Value
Polycarbonate	*n@532 nm*	1.5917
Corrective lens	*diopter*	$-3\ m^{-1}$
	f_c	–0.3333 m
	R_1	1.1000 m
	R_2	0.1672 m

Optics EXPRESS

2.4 Projection lens

Referring to Fig. 2, a 4-element projection lens design, consisting of four different lenses, is adopted. Once the distances s_1 and s_2 are predefined—say 3.8 mm and 20 mm, respectively—by using Eqs. (3) and (4), the image distance S″ and lateral magnification m can be calculated as a function of the diopter of projection lens P_p, as shown in Figs. 4 and 5, respectively. It can be seen that when P_p approaches 278.92 m^{-1}, at which the focal length of projection lens is close to s_1, the image distance will be the infinity. In order for the image to be a magnified virtual image, P_p has to be less than 278.92 m^{-1}—or in other words, the microdisplay should be placed within or nearby the focal length of projection lens. If the target value of image distance S″ is set as 3 m, this will roughly correspond to P_p = 278.35 m^{-1} and m = 604.32.

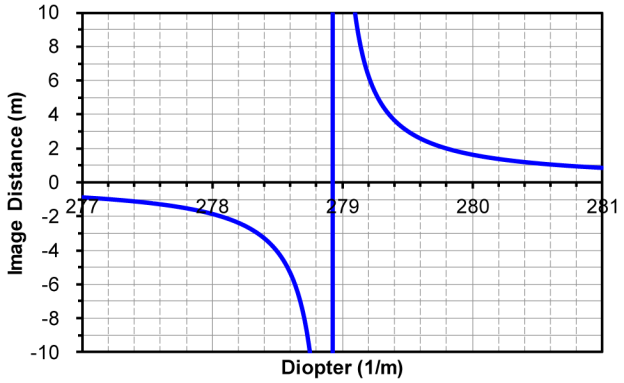

Fig. 4. Image distance versus the diopter of projection lens. It can be seen that when P_p approaches 278.92 m^{-1}, at which the focal length of projection lens is close to s_1, the image distance will be the infinity.

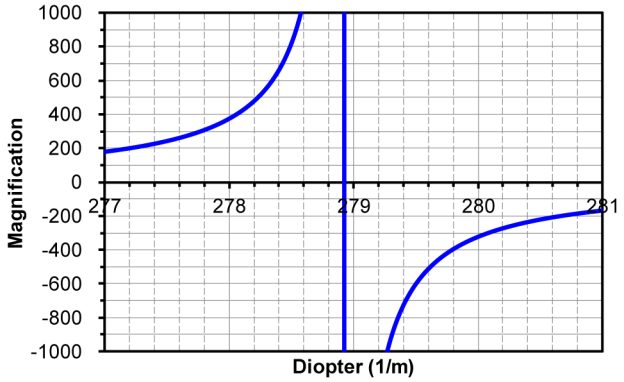

Fig. 5. Lateral magnification versus the diopter of projection lens. If the target value of image distance S″ is set as 3 m, this will roughly correspond to P_p = 278.35 m^{-1} and m = 604.32.

2.5 Volume hologram

Volume hologram plays a critical role in our solution, as it would significantly affect FOV and overall light utilization. Whereas it is considered as a spherical mirror for tracing light rays as above, its diffractive properties have to be analyzed using the physical optics—*e.g.* Fourier modal method [22–24]—rather than the geometrical optics. The design of volume hologram shall follow from the Bragg's law, which is expressed as

Optics EXPRESS

$$\sin\theta_B = \frac{n\lambda}{2\Lambda} \tag{5}$$

$$\Lambda = \frac{\lambda_c}{2\sin\left(\frac{\theta_r - \theta_o}{2}\right)} \tag{6}$$

$$\sin\theta_B = \frac{n\lambda}{\lambda_c}\sin\left(\frac{\theta_r - \theta_o}{2}\right) \tag{7}$$

where θ_B denotes the Bragg angle, n is a positive integer, λ is the incident wavelength in the free space, Λ is the period of hologram, λ_c is the construction wavelength, θ_r and θ_o are the incident angles of reference and object waves, respectively. For achieving full-color volume hologram, wavelengths of red (R), green (G), and blue (B) colors are supposed to match with the same Bragg angle. To satisfy this condition when n = 1, it requires that $\lambda \cdot sin((\theta_r-\theta_o)/2)/\lambda_c$ be a constant. For achieving wide-angle volume hologram, different Bragg angles are supposed to match with the same incident and construction wavelengths. To satisfy this condition when n = 1, it requires that $sin(\theta_B)/sin((\theta_r-\theta_o)/2)$ be a constant. Since a single hologram could only satisfy one Bragg's condition [25], to achieve either full-color or wide-angle, multiplexing or stacking of multiple holograms is inevitable.

3. Results and discussion

3.1 Simulation settings

Our simulation is implemented with the softwares Code V (Synopsys) and VirtualLab (Wyrowski Photonics). The former deals with the ray tracing for analyzing the imaging properties, including MTF, distortion, and imaging simulation. Although Code V could handle several types of gratings by using Kogelnik's coupled-wave theory [26], for a more exact analysis, VirtualLab is used separately for calculating the diffraction efficiency (DE) of volume holograms.

Figure 6 plots a two-dimensional (2D) view of our NED, with the numbering of all surfaces being labelled. A 0.47″ microdisplay with an aspect ratio of 16:9 is employed. According to the design rules said before, we could create an initial structure by presetting the parameters for each object. Then, an optimization, whose error function type is set as transverse ray aberration [27], is carried out by constraining the effective focal length f_e of the whole system as the desired value—i.e. 17.56 mm—and distortion less than 1%. The parameters after the optimization are listed in Table 2. Besides, more detailed parameters for defining aspherical surfaces are listed in Table 3.

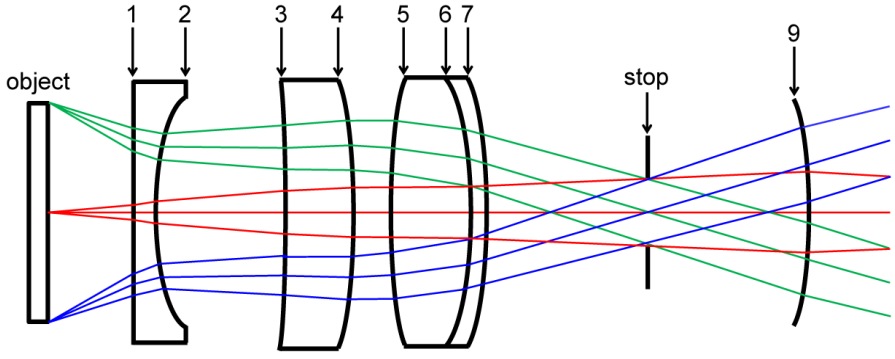

Fig. 6. 2D view of the proposed NED. The numbering of all surfaces is labelled either as their original names or as numbers.

Optics EXPRESS

Table 2. Optimized parameters for the proposed NED

Surface	Surface type	Radius (mm)	Thickness (mm)	Refractive index[a]
object	sphere	infinity	3.7909	
1	sphere	infinity	0.7737	1.62
2	asphere	8.2969	5.7721	
3	asphere	–53.6892	3.0837	1.62
4	asphere	–23.3113	1.5885	
5	sphere	25.4048	3.4815	1.62
6	sphere	–14.2823	0.7737	1.70
7	sphere	–16.7967	11.6048	
stop	sphere	Infinity	8.5578	
9	sphere	–167.18	272.1070	
image	sphere	Infinity	–0.3095	

[a]Refractive index is left empty when the medium is air.

Table 3. Parameters for aspherical surfaces

Surface	Y curvature (mm)	Y radius (mm)	Conic constant (K)	4th order coefficient (A)	6th order coefficient (B)	8th order coefficient (C)
2	0.12053	8.29685	0	0.000313	–3.06E-06	7.98E-08
3	–0.01863	–53.6892	0	0.000105	–1.72E-06	1.24E-07
4	–0.04290	–23.3113	0	5.58E-05	–1.50E-06	7.20E-08

3.2 Diffraction efficiency

In order to realize a full-color display, the wavelength multiplexing is employed. From Eq. (7), three volume holograms can be constructed to reflect R/G/B colors, as defined in Table 4, where d is the thickness, Δn denotes the refractive index modulation—the difference between the maximum and minimum refractive indices, θ_r is 0°—coincident with the normal of the hologram center—and $\theta_o = \theta = 50°$—approximated by assuming s_2 = 20.16 mm and s_3 = 12.96 mm and that s_2 and s_3 would form a right triangle, as shown in Fig. 1. It should be noticed that s_3 is a variable, as the headset where NED is mounted must be adjustable. In order to broaden the angular bandwidth, the angular multiplexing is employed. Similarly, three volume holograms can be constructed to exhibit different Bragg angles, as defined in Table 5. Following the Fourier modal method, individual DEs $\eta_{R/G/B}$ for each hologram are calculated with respect to the wavelengths and incident angles, respectively, as shown in Fig. 7 and Fig. 8. When three holograms are multiplexed, the overall DE η shall be written as

$$\eta = \eta_1 + \eta_2 + \eta_3 - \eta_1\eta_2 - \eta_1\eta_3 - \eta_2\eta_3 + \eta_1\eta_2\eta_3 \tag{8}$$

For wavelength multiplexing, the wavelength bandwidths of R/G/B colors for individual DE>10% are 13 nm (637~649 nm), 12 nm (536~547 nm), and 14 nm (462~475 nm), respectively. For angular multiplexing of green color, the angular bandwidth for overall DE>10% is 33° (36~68°).

Optics EXPRESS

Table 4. Parameters of volume holograms used for wavelength multiplexing

Object	Parameter	Value
Volume hologram R	d	30 μm
	Δn	0.04
	λ_c	633 nm
	θ_r	0°
	θ_o	50°
Volume hologram G	d	30 μm
	Δn	0.04
	λ_c	532 nm
	θ_r	0°
	θ_o	50°
Volume hologram B	d	30 μm
	Δn	0.04
	λ_c	460 nm
	θ_r	0°
	θ_o	50°

Table 5. Parameters of volume holograms used for angular multiplexing

Object	Parameter	Value
Volume hologram G1	d	30 μm
	Δn	0.04
	λ_c	532 nm
	θ_r	0°
	θ_o	39°
Volume hologram G2	d	30 μm
	Δn	0.04
	λ_c	532 nm
	θ_r	0°
	θ_o	50°
Volume hologram G3	d	30 μm
	Δn	0.04
	λ_c	532 nm
	θ_r	0°
	θ_o	60°

Optics EXPRESS

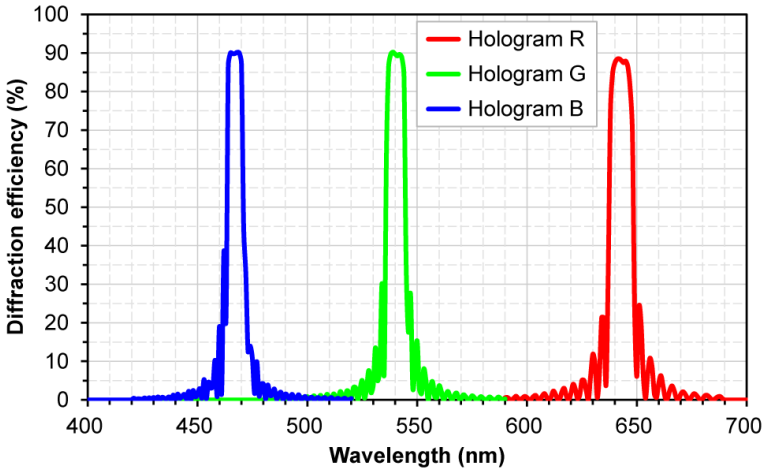

Fig. 7. Calculated DE with respect to wavelengths. For wavelength multiplexing, the wavelength bandwidths of R/G/B colors for individual DE>10% are 13 nm (637~649 nm), 12 nm (536~547 nm), and 14 nm (462~475 nm), respectively.

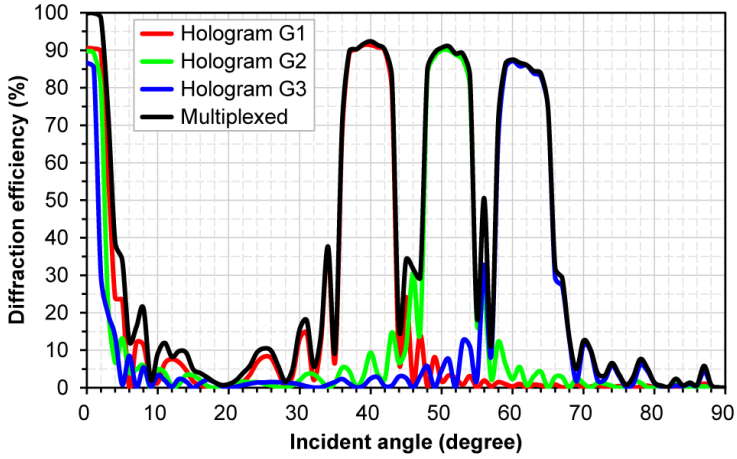

Fig. 8. Calculated DE with respect to incident angles. For angular multiplexing of green color, the angular bandwidth for overall DE>10% is 33° (36~68°).

3.3 Field of view

FOV of our NED is defined as the angular extent of the image of microdisplay that is observed by the fixed eyes. It may be measured horizontally, vertically, or diagonally, and it could also be directly calculated as follows [27]

$$FOV = 2 \cdot arc\tan\left(\frac{d_m}{2f_e}\right) \tag{9}$$

where d_m represents the size of microdisplay measured in a given direction. For our case, the diagonal FOV is approximately 38°—or equivalently 33° measured horizontally—which well matches with the above angular bandwidth of the multiplexed volume holograms.

3.4 Modulation transfer function

By computing Fourier transform of the line spread function, the diffraction MTFs of real and virtual images at the central and marginal angles are plotted in Fig. 9(a) and Fig. 9(b),

Optics EXPRESS

respectively, where MTFs of real images for all angles are above 0.4 at 150 cycles/mm, and MTFs of virtual images for all angles are above 0.4 at 6 cycles/mm.

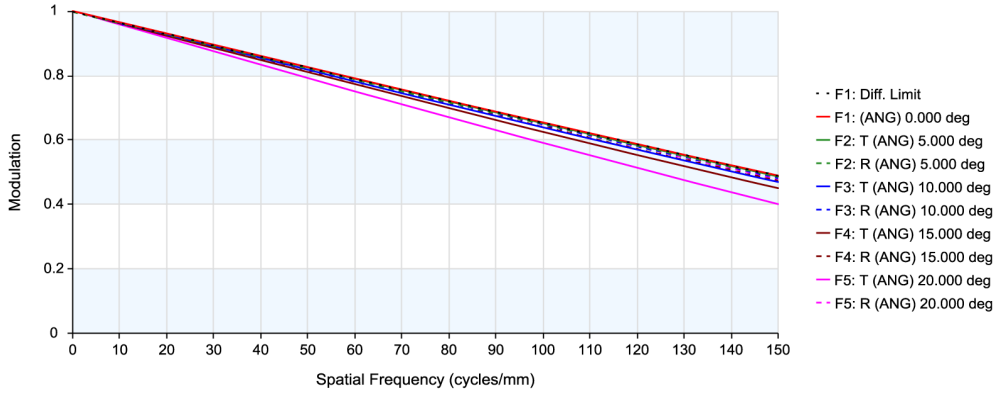

(a)

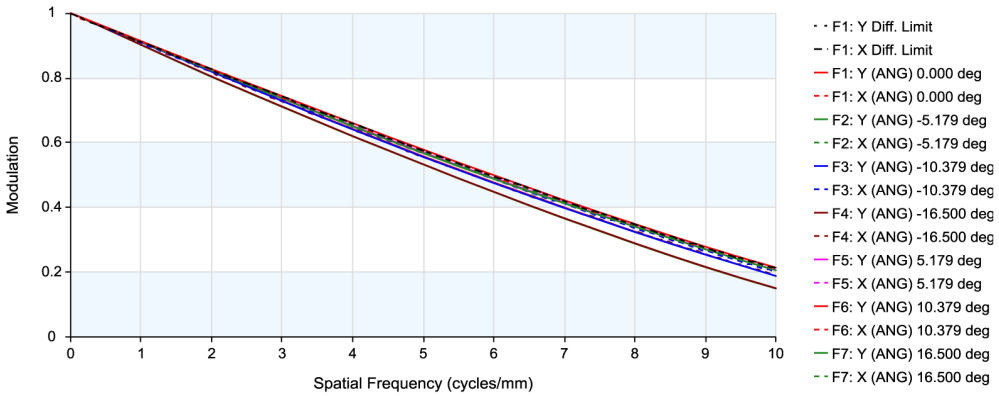

(b)

Fig. 9. Calculated MTFs of (a) real and (b) virtual images. For real images, MTFs for all angles are above 0.4 at 150 cycles/mm. For virtual images, MTFs for all angles are above 0.4 at 6 cycles/mm.

3.5 Distortion

Distortion grids of real and virtual images, defined as the displacement of image height or ray location, are plotted in Fig. 10(a) and Fig. 10(b), respectively, where distortion of real images is less than 0.15%, and distortion of virtual images is less than 0.63%.

Optics EXPRESS

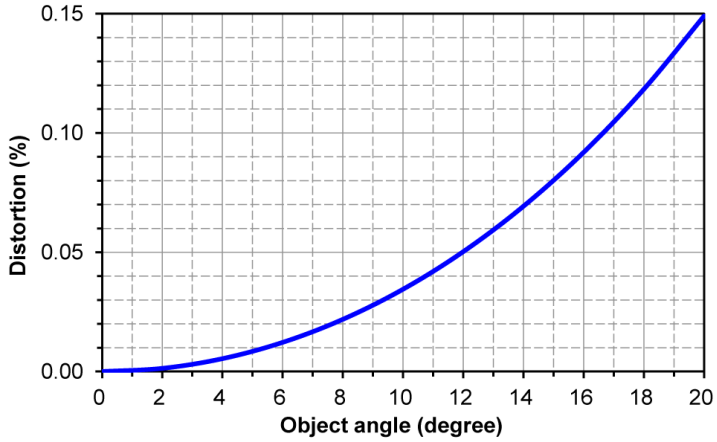

(a)

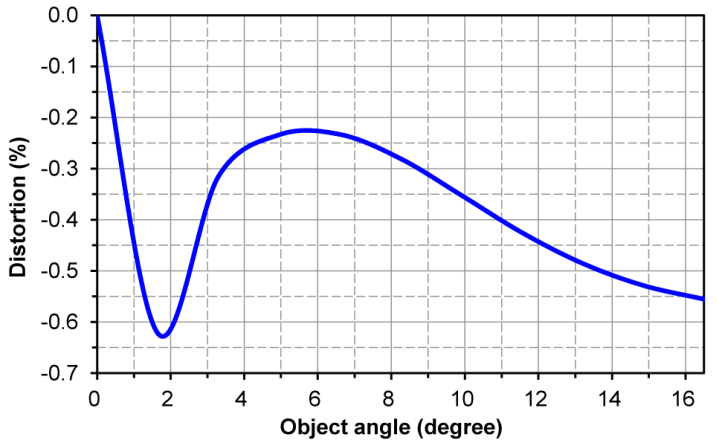

(b)

Fig. 10. Calculated distortion grids of (a) real and (b) virtual images. For real images, distortion is less than 0.15%. For virtual images, distortion is less than 0.63%.

3.6 Simulated imaging

For a qualitative analysis of imaging quality, both real and virtual images are visualized from the imaging simulation that takes into account the effects of distortion, aberration blurring, diffraction blurring, and relative illumination, as shown in Fig. 11(b) and Fig. 11(c). By comparing the original and simulated images, it can be seen that the distortion is almost unnoticeable, while the brightness is reduced and blurring is more apparent for the virtual image, which agrees with the foregoing results.

Optics EXPRESS

(a) (b) (c)

Fig. 11. (a) Original, (b) real, and (c) virtual images. By comparing the original and simulated images, it can be seen that the distortion is almost unnoticeable, while the brightness is reduced and blurring is more apparent for the virtual image, which agrees with the foregoing results.

4. Conclusion

A compact design of see-through NED, featuring a pair of corrective lenses coated with multiplexed volume holograms, has been proposed. Based on the simulation, its optical performance including DE, FOV, MTF, and distortion has been studied. By eliminating the need for extra glasses or contact lens, this type of see-through NED could be particularly appealing to the users who are more or less visually impaired. In addition to myopia, our future work will extend to hyperopia, presbyopia, astigmatism, and combinations of different refractive anomalies.

Funding

National Natural Science Foundation of China (NSFC) (61307028).